LETTER

doi:10.1038/nature18949

Extending the lifetime of a quantum bit with error correction in superconducting circuits

Nissim Ofek[1]*, Andrei Petrenko[1]*, Reinier Heeres[1], Philip Reinhold[1], Zaki Leghtas[1]†, Brian Vlastakis[1], Yehan Liu[1], Luigi Frunzio[1], S. M. Girvin[1], L. Jiang[1], Mazyar Mirrahimi[1,2], M. H. Devoret[1] & R. J. Schoelkopf[1]

Quantum error correction (QEC) can overcome the errors experienced by qubits[1] and is therefore an essential component of a future quantum computer. To implement QEC, a qubit is redundantly encoded in a higher-dimensional space using quantum states with carefully tailored symmetry properties. Projective measurements of these parity-type observables provide error syndrome information, with which errors can be corrected via simple operations[2]. The 'break-even' point of QEC—at which the lifetime of a qubit exceeds the lifetime of the constituents of the system—has so far remained out of reach[3]. Although previous works have demonstrated elements of QEC[4–16], they primarily illustrate the signatures or scaling properties of QEC codes rather than test the capacity of the system to preserve a qubit over time. Here we demonstrate a QEC system that reaches the break-even point by suppressing the natural errors due to energy loss for a qubit logically encoded in superpositions of Schrödinger-cat states[17] of a superconducting resonator[18–21]. We implement a full QEC protocol by using real-time feedback to encode, monitor naturally occurring errors, decode and correct. As measured by full process tomography, without any post-selection, the corrected qubit lifetime is 320 microseconds, which is longer than the lifetime of any of the parts of the system: 20 times longer than the lifetime of the transmon, about 2.2 times longer than the lifetime of an uncorrected logical encoding and about 1.1 longer than the lifetime of the best physical qubit (the $|0\rangle_f$ and $|1\rangle_f$ Fock states of the resonator). Our results illustrate the benefit of using hardware-efficient qubit encodings rather than traditional QEC schemes. Furthermore, they advance the field of experimental error correction from confirming basic concepts to exploring the metrics that drive system performance and the challenges in realizing a fault-tolerant system.

Implementing QEC in the laboratory is challenging, requiring a complex system with many qubits. Even for a perfectly realized QEC system of finite size, there will always be unrecoverable errors or failure modes, resulting in an exponential decay of the information over time. In fact, error correction first introduces a hardware overhead penalty, because an uncorrected logical qubit consisting of n physical qubits (for typical first-order codes $n \approx 5$–10; ref. 22) will experience decoherence that is of order n times faster. A central goal of QEC is to suppress the naturally occurring errors and surpass the break-even point, at which the lifetime gain due to error correction is larger than this overhead penalty. These considerations motivate exploring a hardware-efficient approach to QEC, with which it may be more tractable to not only overcome the entire overhead, but to pinpoint the leading limitations to fault-tolerance.

The encoding of logical states as superpositions of Schrödinger-cat states (hereafter, 'cat code') that we implement here is a hardware-efficient scheme that requires fewer physical resources and introduces fewer error mechanisms than do traditional QEC proposals. Designed to operate within a continuous-variable framework[23], the cat code exploits the fact that a coherent state $|\alpha\rangle$ is an eigenstate of the resonator lowering operator $\hat{a}$: $\hat{a}|\alpha\rangle = \alpha|\alpha\rangle$. Using a logical basis comprised of superpositions of cat states, which are eigenstates of photon-number parity, the cat code requires just a single ancilla to monitor the dominant error due to single photon loss induced by resonator energy damping. This error channel gives rise to two effects: deterministic energy decay of the resonator field to vacuum and the stochastic application of $\hat{a}$, which results in a change of photon-number parity of any state within the cat code. The former becomes a limiting factor only at small resonator field amplitudes when coherent state overlap can no longer be neglected and can be addressed through either dissipative pumping approaches[24] or unitary gates. The latter, photon loss, is accompanied by phase shifts of $\pi/2$ about the Z_c axis within the logical space, indicating that by monitoring photon parity as the error syndrome we adhere to the prescriptions for error correction by translating single photon loss into a unitary operation on the encoded state[18,19] (Fig. 1):

$$\hat{a}\left(c_0\left|C_\alpha^+\right\rangle + c_1\left|C_{i\alpha}^+\right\rangle\right) \propto \frac{c_0}{\sqrt{2}}\left(\left|\alpha\right\rangle - \left|-\alpha\right\rangle\right) + i\frac{c_1}{\sqrt{2}}\left(\left|i\alpha\right\rangle - \left|-i\alpha\right\rangle\right)$$
$$= c_0\left|C_\alpha^-\right\rangle + ic_1\left|C_{i\alpha}^-\right\rangle$$

where c_0 and c_1 are arbitrary coefficients satisfying $|c_0|^2 + |c_1|^2 = 1$ and $|C_{(i)\alpha}^{\pm}\rangle = (|(i)\alpha\rangle \pm |-(i)\alpha\rangle)/\sqrt{2}$ (the normalization factor $\sqrt{2}$ holds in the limit of large α (refs 17 and 18)). By detecting photon jumps in real-time with quantum non-demolition parity measurements[21], we learn how the phase relationship between the basis states changes, thereby protecting the encoded qubit from the dominant error channel of the system. The rate of photon jumps scales linearly with the average photon number $\bar{n}$ (ref. 17), which exactly mirrors the aforementioned overhead faced by traditional QEC codes[22,25]. Thus, when implementing the cat code, a central figure of merit when assessing the performance of the QEC system will be the degree to which we can overcome the encoding overhead with the application of fast, repeated parity measurements in time.

We use a 3D circuit quantum electrodynamics (QED) architecture[26] consisting of a single transmon qubit coupled to two waveguide resonators[21,27]. The transmon is used as an ancilla both to provide the error syndrome and to encode and decode the logical states (Supplementary Information, section 3). One resonator stores the logical states while the other is used for ancilla readout and control. The dominant storage–ancilla interaction terms are described by the following Hamiltonian:

$$\hat{H}/\hbar = \omega_s\hat{a}^\dagger\hat{a} + \left(\omega_a - \chi_{sa}\hat{a}^\dagger\hat{a}\right)\left|e\right\rangle\left\langle e\right| - \frac{K}{2}\hat{a}^{\dagger 2}\hat{a}^2$$

with $|e\rangle\langle e|$ the ancilla excited state projector, ω_s and ω_a the storage resonator (henceforth the resonator) and ancilla transition frequencies,

[1]Departments of Physics and Applied Physics, Yale University, New Haven, Connecticut 06510, USA. [2]QUANTIC team, INRIA de Paris, 2 Rue Simone Iff, 75012 Paris, France. †Present address: Centre Automatique et Systèmes, Mines-ParisTech, PSL Research University, 60, boulevard Saint-Michel, 75006 Paris, France.
*These authors contributed equally to this work.

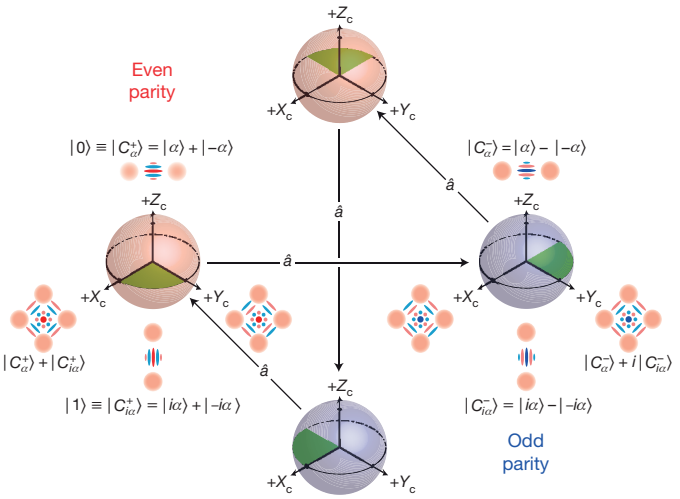

Figure 1 | The cat-code cycle. In the logical encoding of $|0\rangle \equiv |C^{\pm}_{\alpha}\rangle = |\alpha\rangle \pm |-\alpha\rangle$ and $|1\rangle \equiv |C^{\pm}_{i\alpha}\rangle = |i\alpha\rangle \pm |-i\alpha\rangle$ (normalizations omitted), the two '2-cats' $|C^{\pm}_{\alpha}\rangle$ and $|C^{\pm}_{i\alpha}\rangle$ are eigenstates of either even (+) or odd (−) photon-number parity (an '*n*-cat' is a superposition of *n* coherent states). For large enough $|\alpha|$ they are effectively orthogonal to one another. In this basis, the states along the logical axes $+X_c$ and $+Y_c$ are both '4-cats' of even or odd parity as well. The different patterns in the fringes of their cartoon Wigner functions signify the different phase relationship between the basis states. These features allow one to store a qubit in a superposition of 2-cats, $|\psi\rangle = c_0|C^{\pm}_{\alpha}\rangle + c_1|C^{\pm}_{i\alpha}\rangle$, and at the same time monitor the parity as the error syndrome without learning anything about c_0 or c_1, the arbitrary coefficients satisfying $|c_0|^2 + |c_1|^2 = 1$. In this example, we choose to encode $|0\rangle$ and $|1\rangle$ in the even-parity basis, although the odd basis can equally be chosen. The loss of a single photon changes not just the parity of the basis states (red shading, even; blue shading, odd), but the phase relationship between them by a factor of *i* as well: $\hat{a}(c_0|C^+_\alpha\rangle + c_1|C^+_{i\alpha}\rangle) = c_0|C^-_\alpha\rangle + ic_1|C^-_{i\alpha}\rangle$. Therefore, after one photon jump, one finds the initial qubit rotated by $\pi/2$ about the logical Z_c axis. With each subsequent application of $\hat{a}$, the encoded state cycles between the even- and odd-parity subspaces, while, owing to each consequent multiplication of the coefficient c_1 by *i*, the encoded information rotates about the Z_c axis by $\pi/2$, as indicated by the rotation of the green shaded slice. Between the stochastic applications of $\hat{a}$, the cat states deterministically decay towards vacuum: $\alpha \rightarrow \alpha e^{-\kappa t/2}$ (not depicted here), indicating that the logical basis changes in time.

respectively, $\chi_{sa}/(2\pi) \approx 1.95$ MHz the dispersive frequency shift, $K/(2\pi) \approx 4.5$ kHz the resonator anharmonicity, or Kerr, and $\hbar$ is the reduced Planck constant. The ancilla has coherence times $T_1 \approx 35\,\mu$s and $T_2 \approx 13\,\mu$s; the resonator has a single-photon Fock state relaxation time $\tau_c \approx 250\,\mu$s and coherence time $T_2^c \approx 330\,\mu$s. To perform high-fidelity single-shot measurements of the ancilla[28], we set the readout resonator to have a 1-MHz bandwidth and use a nearly quantum-limited phase-preserving amplifier, the Josephson parametric converter (JPC)[29], as the first stage of amplification, which allows for a readout fidelity of 99.3%. The error syndrome is measured using a Ramsey-style pulse sequence consisting of two $\pi/2$ pulses applied on the ancilla and separated in time by $\pi/\chi_{sa} \approx 250$ ns (ref. 30). The subsequent ancilla projective readout takes about 700 ns, which includes integration times, cable latencies and feedback delays. A change in the ancilla state after the Ramsey mapping indicates a change in parity, or the loss of one photon (assuming negligible photon excitation) with 98.5% fidelity (Supplementary Information, section 1). The total duration of each error syndrome measurement is just 1 μs, or approximately 0.8% of the average time between photon jumps for cat states with $\bar{n}$=2.

We use a new real-time controller designed to execute programs for quantum control (Supplementary Information, section 5). Every repetition of the program (Fig. 2a–d) begins with the controller encoding one of the six cardinal points on a Bloch sphere in the even logical basis states, enough to perform process tomography of the full QEC system[2]. The number of syndrome measurements and the waiting time t_w between them is set to an optimal value to balance the risk of missing photon jumps and the possibility of measurement back-action on the resonator state due to ancilla T_1 (Supplementary Information, section 4; more details below); for cat states of $\bar{n} \approx 3$, $t_w \approx 13\,\mu$s. The program uses a state machine for adaptive parity monitoring, in which the sign of the second $\pi/2$ pulse in the parity mapping is chosen in real-time to maximize the probability of measuring the ancilla in its ground state $|g\rangle$; this improves measurement reliability by decreasing the probability that the state of the ancilla will change during measurement.

The program stores in memory a record of '0's (no error) and '1's (error) that specifies the monitoring history; Fig. 2b shows the four possibilities for two steps: {00, 01, 10, 11} with probabilities {70.4%, 13.7%, 11.8%, 4.1%}. The asymmetry in the occurrence of 01 and 10 is due to parity measurement infidelity and is well-modelled by a Bayesian analysis (Supplementary Information, section 7). Conditioned on obtaining one of these four records, Wigner tomography provides a striking visual demonstration of the cat code in action. Interference fringes, signatures of quantum coherence[17], continue to be sharp and extremal as the program proceeds in time, as compared with the case of performing no parity monitoring. At each point in the program the tomograms agree well in parity contrast, phase and amplitude as seen in simulations. These levels of predictability highlight the advantages of this hardware-efficient scheme: knowing the Hamiltonian parameters and the measurement fidelity of a single error syndrome is sufficient to encapsulate the evolution of an error-corrected logical qubit.

Two further applications of feedback are necessary to maximize the performance of the QEC system. Owing to the non-commutativity of the Kerr Hamiltonian $\frac{K}{2}\hat{a}^{\dagger 2}\hat{a}^2$ and $\hat{a}$, a photon jump results in a phase shift of the resonator state in phase space proportional to *K* and the jump time t_j: $\theta_K = Kt_j$ (ref. 18). The controller must therefore use the monitoring history, which provides a best-estimate of t_j, to consolidate trajectories of equal error number, yet different error timestamp, into a single effective resonator state in real-time; for example, before decoding, 01 and 10 become a single '1 error' state. The controller also decides in real-time to apply a different set of decoding pulses on the basis of the final parity. Figure 2c shows qubit state tomography of the ancilla after decoding, but before correction, conditioned on the number of errors. The rotation of the six cardinal points by $\pi/2$ for one error and π for two errors indicates that the cat code successfully maps photon-loss errors in the resonator onto a unitary operation on the encoded qubit. Upon completion of execution of the program, the knowledge of how many errors occurred is equivalent to having corrected the state. Although aligning the Bloch spheres of all error trajectories to the same orientation requires a simple phase adjustment on the ancilla drive in the decoding sequence, in this example we instead choose to show the performance of each error case individually. The program thus returns the corrected qubit, now stored again in the ancilla, completing the full QEC cycle.

We benchmark the performance of our QEC system by performing process tomography of the QEC system. We use the chi matrix representation for a single qubit[2], in which state tomography of the output density matrix ρ_{fin} is used to calculate the measured, complex 4×4 chi matrix X^M. The fidelity $F = \mathrm{tr}(X^M X_0)$ is defined as the overlap of X^M with X_0, the chi matrix for the identity operator $\hat{I}$, the ideal case in which a QEC system corrects a state perfectly. Shown in Fig. 2e are the process matrices for the QEC program demonstrated in Fig. 2a–d. The form of X^M_j (X^M for $j = 0$, 1 and 2 errors) matches the process matrix for ideal rotations about the *Z* axis (defined by the Pauli matrix σ_z) by $j\pi/2$, $X_{j\pi/2}$. Signatures of developing incoherent mixture are evident from the non-zero values in all diagonal elements.

Moving to an initial encoding size of $\bar{n}_0$=2 to reduce the probability of photon jumps, we implement the cat code with up to six syndrome measurements over approximately 110 μs (Fig. 3a). As in Fig. 2b, each repetition is separated by an optimized waiting time that depends on

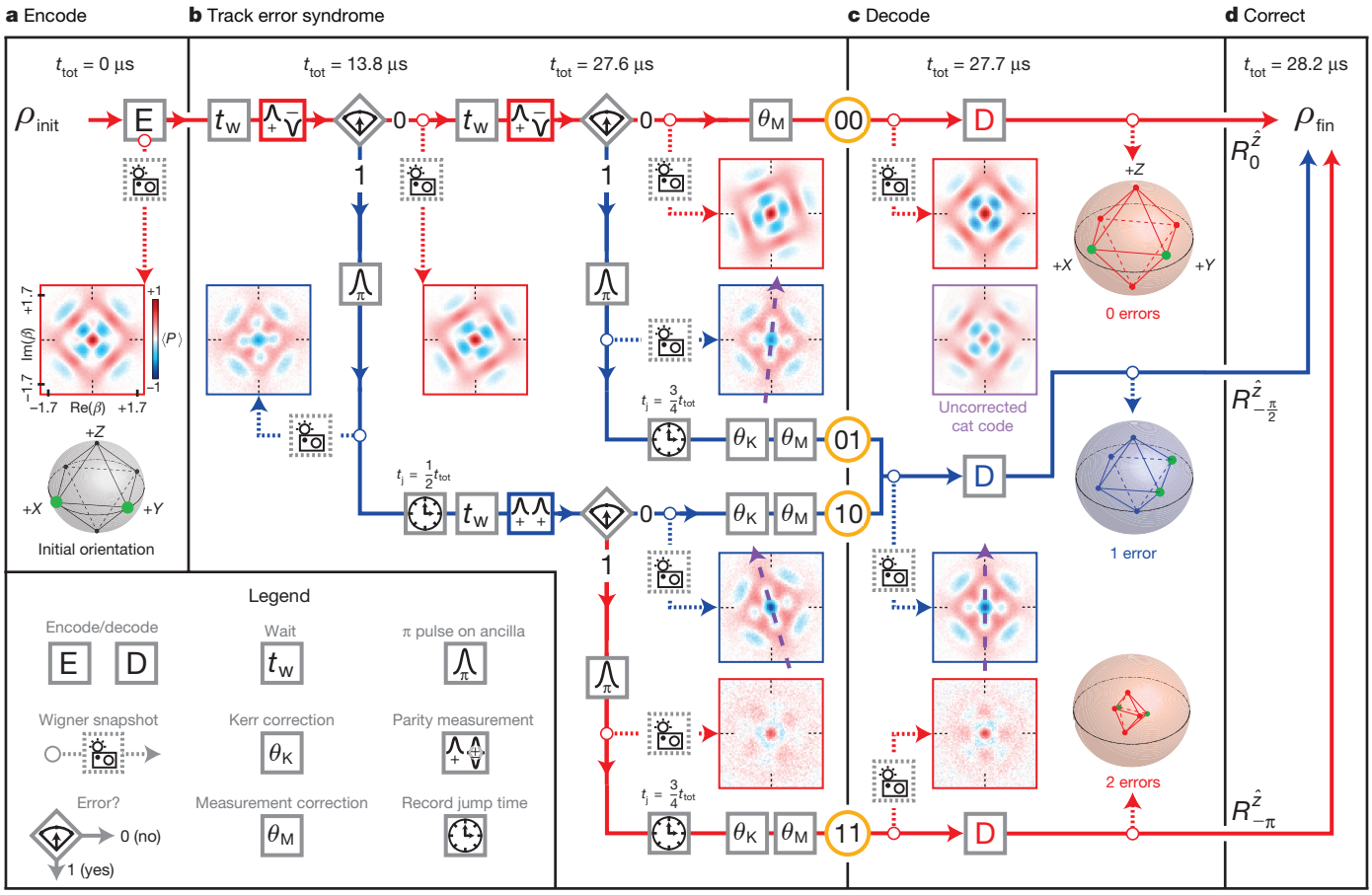

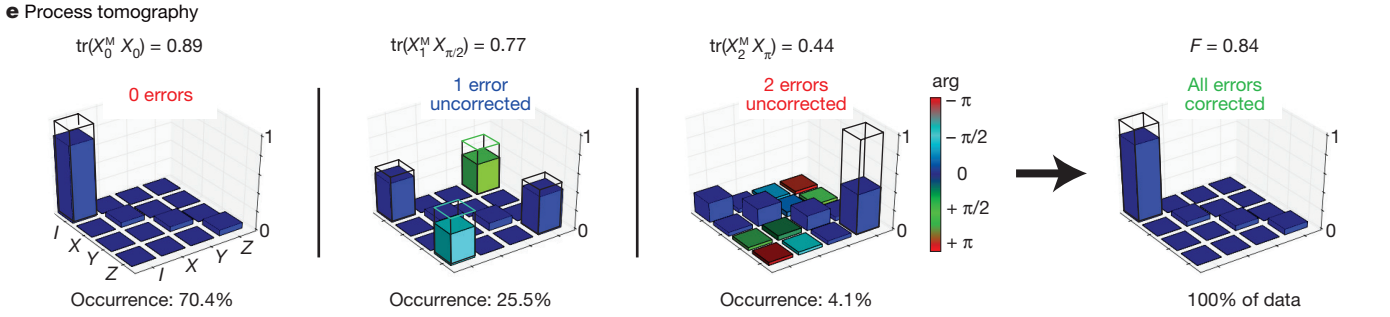

Figure 2 | Example of a two-step quantum trajectory executed by the QEC state machine. a, Six cardinal points on the Bloch sphere ρ_{init} are encoded ('E') from the ancilla onto even-parity resonator states; green markers indicate the initial coordinate-system orientation. A 'Wigner [tomography] snapshot' is shown for $\frac{1}{\sqrt{2}}(|0\rangle - |1\rangle) \rightarrow \frac{1}{\sqrt{2}}(|C_\alpha^+\rangle - |C_{i\alpha}^+\rangle)$; $\bar{n}_0$=3; β is the amplitude of varying coherent displacements ($\hat{D}_\beta|0\rangle_f = |\beta\rangle$) and the average parity $\langle P\rangle = \langle \hat{D}_\beta^\dagger \hat{P} \hat{D}_\beta\rangle$, where $\hat{P} = e^{i\pi a^\dagger a}$. **b**, A state machine for adaptive parity monitoring with delays $t_w \approx 13$ µs between each measurement. 'Parity measurement' rectangles show the Ramsey sequence that maps even [+/−] (odd [+/+]) parity onto ancilla $|g\rangle$ ($|e\rangle$); the + or − specifies the sign of the π/2 pulse. Diamonds indicate branching on ancilla measurement (0 → no error, $|g\rangle$; 1 → error, $|e\rangle$); 'π pulse on ancilla' rectangle indicates ancilla reset ($|e\rangle \rightarrow |g\rangle$); clocks indicate recording of the error time t_j. Dashed purple arrows emphasize the phase difference between 10 and 01 due to θ_K. Rotations θ_M are due to cross-Kerr interactions between the readout and storage resonators during ancilla measurements. The parity (Wigner tomogram origin) matches the best estimate (border colour); tomograms match the expected resonator state as seen in simulations. **c**, The feedback aligns all states by changing the phase of subsequent resonator drives (for example, for Wigner tomography or decoding pulses) to account for θ_K and θ_M. Ancilla tomography after decoding shows the expected rotations of π/2 per error about Z (green markers). Different decoding pulses ('D') are chosen in real-time depending on the parity of the final state. **d**, The correction to obtain the final state ρ_{fin} is made via coordinate system rotations ($R^{\hat{z}}$, where $\hat{z}$ is the qubit axis defined by Pauli matrix σ_z) by 0 (for 0 errors), −π/2 (for 1 error) or −π (for 2 errors) in software. **e**, Process tomography results for j = 0, 1 and 2 errors before correction. Ideal $X_{j\pi/2}$ process matrices are shown in wire-outlined bars. Experimental data for X_j^M are shown in solid bars; the values are complex numbers with the amplitude on the vertical axis and an argument specified by the bar colour. Amplitudes of less than 0.01 are not depicted. Process tomography after correction is shown to the right of the arrow. I, the identity matrix; F, fidelity.

the average photon number in the resonator, starting at $t_w \approx 15$ µs and increasing after each subsequent step up to $t_w \approx 25$ µs to account for the decay of the average photon number. Without post-selection, the cat code outperforms the uncorrected transmon with a time constant of exponential decay that is a factor of about 20 higher, indicating that although the coupling between the resonator and transmon is always on, the efficient extraction of error syndromes using an ancilla with inferior coherence properties still allows for substantial gains in lifetime. Moreover, the cat code surpasses the decay of the uncorrected cat code by a factor of about 2.2, demonstrating that applying error correction to the logical encoding makes up for the faster error rates introduced by the hardware overhead. The palpable difference in

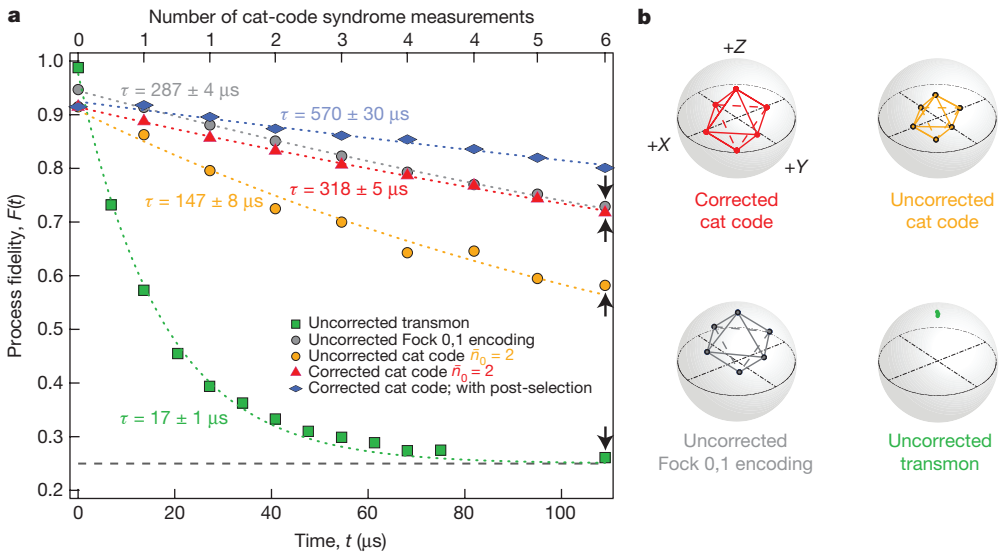

Figure 3 | QEC process tomography. a, To implement QEC, we redundantly encode the qubit in cat states ($\bar{n}_0$=2) and pay the required overhead penalty, which is ubiquitous to QEC. This leads initially to worse performance; the process fidelity ($F(t)$) of the uncorrected cat code (orange circles), where cat states are left to decay freely between encoding and decoding, exhibits faster decay as compared to the Fock states $|0\rangle_f$ and $|1\rangle_f$ (grey circles). Substantial improvements in performance are realized with the full QEC system; the corrected cat code (red triangles) surpasses the uncorrected transmon (green squares) by a factor of about 20, makes up for the QEC overhead by a factor of about 2.2, and offers an improvement over the Fock-state encoding by a factor of about 1.1. With only high-confidence trajectories (blue diamonds), the decay time τ increases to $\tau > 0.5$ ms. The top axis indicates the number of syndrome measurements used for each point in the corrected cat code. Cat code data: 100,000 averages per point; transmon, Fock states: 50,000 averages per point; error bars are smaller than marker sizes. Although no data exhibits strictly single-exponential decay, all curves are well modelled by $F(t) = 0.25 + Ae^{-t/\tau}$ (dotted lines), with τ the decay time of the specific qubit storage scheme and A a fitting constant that is ideally equal to 0.75. $F = 0.25$ (grey dashed line) implies a complete loss of information. Uncertainties are given by the errors (on τ) in the fit. Fluctuations in the uncorrected cat code are explained by the Kerr effect and are reproduced in simulation. **b**, State tomography after approximately 110 μs (corresponding to black arrows in **a**). Transmon and Fock-state Bloch spheres show amplitude damping. Bloch sphere shrinking for the cat code is well-characterized by a depolarization channel. The system substantially benefits from QEC, as seen from the greater definition of each cardinal point in the corrected versus uncorrected case.

contrast between the cardinal points of the uncorrected versus the corrected cat codes after approximately 110 μs (Fig. 3b) demonstrates that with a full QEC system we can enhance the lifetime of a qubit without giving preference to any one direction on the Bloch sphere. By decaying with a time constant that exceeds that of the Fock state by a factor of 1.1, this system reaches the break-even point of QEC.

The history of errors also provides us with a valuable measure of confidence that the result of an error syndrome measurement faithfully reflects the actual error history. Indeed, a 'low-confidence' measurement record that suggests two or more consecutive errors (for example, 11 as in Fig. 2c) has a much lower probability of faithfully reflecting the true error trajectory of the resonator state than does a 'high-confidence' record, wherein a 1 is 'confirmed' by a subsequent 0 (Supplementary Information, section 7). If we accept only high-confidence trajectories, still keeping 80% of the data after 100 μs, then we obtain a decay constant of over half a millisecond. The marked improvement we observe when excluding 'low-confidence' trajectories points to parity measurement infidelity, primarily due to ancilla decoherence, as the dominant limitation on cat-code performance.

An overall analysis of the budget for the lifetime gain for our QEC system is shown in Table 1, which lists the dominant avenues of code failure common to any QEC system and encapsulates the challenges one faces in realizing fault-tolerant QEC. Contributions from the first five entries in Table 1 can be suppressed by measuring more quickly and using a quantum filter to estimate the parity at any given time[21], as seen in the column where $t_w \approx 0$ μs. However, errors due to the ancilla T_1 persist regardless of measurement rate. Owing to its dispersive coupling to the resonator, a change in the energy of the ancilla at an unknown time imparts an unknown rotation to the resonator state in phase space; this is the forward propagation of an error. Measuring the syndrome more frequently only increases the likelihood of ancilla-induced dephasing, necessitating the aforementioned optimized

Table 1 | Failure modes of the corrected logical qubit

Failure mode	Dominant source	Maximum rate, $t_w \approx 0$ μs	Optimal rate, $t_w \approx 20$ μs
		Predicted τ	
Double errors	Cavity $\hat{a} \cdot \hat{a}$	40 ms	1.7 ms
Uncorrectable errors	Cavity $\hat{a}^\dagger$	6 ms	6 ms
Readout error	Transmon T_ϕ	7 ms	2 ms
Ancilla preparation	Transmon $\Gamma_\uparrow$	300 ms	900 μs
Undesired couplings	Cavity $\hat{a}^{\dagger 2}\hat{a}^2$	600 ms	3 ms
Forward propagation	Transmon T_1	200 μs	600 μs
Net lifetime	Predicted	200 μs	320 μs
	Measured	-	318 μs
Gain over uncorrected logical qubit		1.4	2.2
Gain over best physical qubit		0.7	1.1

This table shows the predicted decay time constant (τ) of quantum information stored in a corrected logical qubit using the cat-code paradigm under a scenario in which each individual failure mode is the only source of loss. Dominant modes of failure in the cat code are: double errors ($\hat{a}$ followed by $\hat{a}$) between consecutive syndrome measurements separated by a time t_w; possible errors that the cat code does not address, such as additions of a single photon ($\hat{a}^\dagger$); a failed parity mapping resulting from ancilla dephasing (T_ϕ); incorrect ancilla initialization before syndrome measurement resulting from unknown excitations ($\Gamma_\uparrow$) of the ancilla during t_w; undesired couplings that result in dephasing due to Kerr ($\hat{a}^{\dagger 2}\hat{a}^2$); and ancilla decoherence that directly propagates to unrecoverable errors in the resonator state, which is a result of ancilla decay or excitation (T_1). Two different measurement strategies are shown for an initial $\bar{n}_0$=2: as quickly as possible ($t_w \approx 0$ μs) and the optimal monitoring time ($t_w \approx 20$ μs). The lowest two rows show the multiplicative gains of cat-code performance over the decay constants of the uncorrected logical qubit (147 μs) and the best physical qubit of the system (287 μs, Fock states $|0\rangle_f, |1\rangle_f$). These gains reflect the combined effects of all loss channels acting together. We predict all numbers using an analytical model derived in Supplementary Information, section 6, and show that for the net gains the failure modes do not contribute independently. Using the optimal measurement strategy, we find that the predicted gains in lifetime over the uncorrected logical qubit and over the Fock state encoding match the measured performance of the corrected cat code (318 μs) shown in Fig. 3. Lifetimes of at least 6 ms would be possible if the forward propagation of errors from the syndrome measurements were abated.

measurement cadence that sets the delay between syndrome measurements from $t_w \approx 0\,\mu s$ to, on average, $t_w \approx 20\,\mu s$ for $\bar{n}_0 = 2$. We therefore see that when designing a QEC system, sources of decoherence beyond double-errors per round of correction can motivate substantially slower measurement rates. However, because the cat code performs at the break-even point even in the presence of all of these sources of loss, we are optimistic about the prospect of realizing a fault-tolerant QEC system. Indeed, supplementing the cat code with a scheme that abates ancilla back-action promises to allow increased error syndrome measurement rates (a lower t_w) and thus greater gains in lifetime.

Our results show that QEC can actually protect an unknown bit of quantum information, and extend its lifetime by active means. Furthermore, we demonstrate the crucial role of real-time feedback with pulses that depend on the evolution of the quantum system, an addition to the experimental setup that greatly improves error correction performance and allows us to realize the cat code at the break-even point of QEC. Future goals include combining the cat code with mechanisms to re-inflate cat state amplitudes[24] and to equip the parity monitoring protocol to handle changes in ancilla energy, thereby addressing issues of non-fault-tolerance. With such capabilities we can then move beyond using the cat code as a quantum memory only and begin coupling multiple resonators together to demonstrate operations between error-corrected logical qubits[19]. Our results motivate the adoption of hardware-efficient QEC schemes and demonstrate the promise of cat states as a basis for future quantum computing applications.

Received 12 February; accepted 8 June 2016.
Published online 20 July 2016.

1. Shor, P. W. Scheme for reducing decoherence in quantum computer memory. *Phys. Rev. A* **52,** R2493–R2496 (1995).
2. Nielsen, M. & Chuang, I. *Quantum Computation and Quantum Information* (Cambridge Univ. Press, 2010).
3. Devoret, M. H. & Schoelkopf, R. J. Superconducting circuits for quantum information: an outlook. *Science* **339,** 1169–1174 (2013).
4. Cory, D. *et al.* Experimental quantum error correction. *Phys. Rev. Lett.* **81,** 2152–2155 (1998).
5. Knill, E., Laflamme, R., Martinez, R. & Negrevergne, C. Benchmarking quantum computers: the five-qubit error correcting code. *Phys. Rev. Lett.* **86,** 5811–5814 (2001).
6. Chiaverini, J. *et al.* Realization of quantum error correction. *Nature* **432,** 602–605 (2004).
7. Schindler, P. *et al.* Experimental repetitive quantum error correction. *Science* **332,** 1059–1061 (2011).
8. Waldherr, G. *et al.* Quantum error correction in a solid-state hybrid spin register. *Nature* **506,** 204–207 (2014).
9. Taminiau, T. H., Cramer, J., van der Sar, T., Dobrovitski, V. V. & Hanson, R. Universal control and error correction in multi-qubit spin registers in diamond. *Nat. Nanotechnol.* **9,** 171–176 (2014).
10. Cramer, J. *et al.* Repeated quantum error correction on a continuously encoded qubit by real-time feedback. *Nat. Commun.* **7,** 11526 (2016).
11. Pittman, T. B., Jacobs, B. C. & Franson, J. D. Demonstration of quantum error correction using linear optics. *Phys. Rev. A* **71,** 052332 (2005).
12. Aoki, T. *et al.* Quantum error correction beyond qubits. *Nat. Phys.* **5,** 541–546 (2009).
13. Reed, M. D. *et al.* Realization of three-qubit quantum error correction with superconducting circuits. *Nature* **482,** 382–385 (2012).
14. Kelly, J. *et al.* State preservation by repetitive error detection in a superconducting quantum circuit. *Nature* **519,** 66–69 (2015).
15. Córcoles, A. D. *et al.* Demonstration of a quantum error detection code using a square lattice of four superconducting qubits. *Nat. Commun.* **6,** 6979 (2015).
16. Ristè, D. *et al.* Detecting bit-flip errors in a logical qubit using stabilizer measurements. *Nat. Commun.* **6,** 6983 (2015).
17. Haroche, S. & Raimond, J.-M. *Exploring the Quantum: Atoms, Cavities, and Photons* (Oxford Univ. Press, 2006).
18. Leghtas, Z. *et al.* Hardware-efficient autonomous quantum memory protection. *Phys. Rev. Lett.* **111,** 120501 (2013).
19. Mirrahimi, M. *et al.* Dynamically protected cat-qubits: a new paradigm for universal quantum computation. *New J. Phys.* **16,** 045014 (2014).
20. Vlastakis, B. *et al.* Deterministically encoding quantum information using 100-photon Schrödinger cat states. *Science* **342,** 607–610 (2013).
21. Sun, L. *et al.* Tracking photon jumps with repeated quantum non-demolition parity measurements. *Nature* **511,** 444–448 (2014).
22. Steane, A. M. Error correcting codes in quantum theory. *Phys. Rev. Lett.* **77,** 793–797 (1996).
23. Braunstein, S. L. & van Loock, P. Quantum information with continuous variables. *Rev. Mod. Phys.* **77,** 513–577 (2005).
24. Leghtas, Z. *et al.* Confining the state of light to a quantum manifold by engineered two-photon loss. *Science* **347,** 853–857 (2015).
25. Fowler, A. G., Mariantoni, M., Martinis, J. M. & Cleland, A. N. Surface codes: towards practical large-scale quantum computation. *Phys. Rev. A* **86,** 032324 (2012).
26. Wallraff, A. *et al.* Strong coupling of a single photon to a superconducting qubit using circuit quantum electrodynamics. *Nature* **431,** 162–167 (2004).
27. Paik, H. *et al.* Observation of high coherence in Josephson junction qubits measured in a three-dimensional circuit QED architecture. *Phys. Rev. Lett.* **107,** 240501 (2011).
28. Vijay, R., Slichter, D. H. & Siddiqi, I. Observation of quantum jumps in a superconducting artificial atom. *Phys. Rev. Lett.* **106,** 110502 (2011).
29. Bergeal, N. *et al.* Phase-preserving amplification near the quantum limit with a Josephson ring modulator. *Nature* **465,** 64–68 (2010).
30. Bertet, P. *et al.* Direct measurement of the Wigner function of a one-photon Fock state in a cavity. *Phys. Rev. Lett.* **89,** 200402 (2002).

Supplementary Information is available in the online version of the paper.

Acknowledgements We thank K. Sliwa, A. Narla and L. Sun for discussions. This research was supported by the US Army Research Office (W911NF-14-1-0011). A.P. was supported by the National Science Foundation (NSF) (PHY-1309996). S.M.G. acknowledges additional support from NSF DMR-1301798. Facilities use was supported by the Yale Institute for Nanoscience and Quantum Engineering (YINQE), the Yale SEAS cleanroom and the NSF (MRSECDMR 1119826).

Author Contributions A.P. and N.O. performed the experiment and analysed the data. N.O. designed and built the feedback architecture with help from Y.L. under the supervision of R.J.S. and M.H.D. R.H. and P.R. developed the optimal control pulses. M.M., Z.L., L.J., S.M.G. and B.V. provided theoretical support. R.H. and L.F. fabricated the transmon qubit. R.J.S. supervised the project. A.P., N.O., L.F. and R.J.S. wrote the manuscript with feedback from all authors.

Author Information Reprints and permissions information is available at www.nature.com/reprints. The authors declare competing financial interests: details are available in the online version of the paper. Readers are welcome to comment on the online version of the paper. Correspondence and requests for materials should be addressed to A.P. (andrei.o.petrenko@gmail.com), N.O. (nissim.of@gmail.com) or R.J.S. (robert.schoelkopf@yale.edu).